

MEASURING THE STELLAR MASSES OF $Z \sim 7$ GALAXIES WITH SPITZER ULTRAFAINST SURVEY PROGRAM (SURFS UP)

R. E. RYAN JR.², A. H. GONZALEZ³, B. C. LEMAUX⁴, M. BRADAČ⁵, S. CASERTANO², S. ALLEN⁶, B. CAIN⁵, M. GLADDERS⁷,
 N. HALL⁵, H. HILDEBRADT¹⁰, J. HINZ⁹, K.-H. HUANG⁵, L. LUBIN⁵, T. SCHRABBACK¹⁰, M. STIAVELLI², T. TREU^{11,12}, A.
 VON DER LINDEN^{6,13}, D. ZARITSKY⁹

Draft version April 2, 2014

ABSTRACT

We present Spitzer/IRAC observations of nine z' -band dropouts highly magnified ($2 \lesssim \mu \lesssim 12$) by the Bullet Cluster. We combine archival imaging with our Exploratory program (SURFS UP), which results in a total integration time of ~ 30 hr per IRAC band. We detect ($\gtrsim 3\sigma$) in both IRAC bands the brightest of these high-redshift galaxies, with $[3.6] = 23.80 \pm 0.28$ mag, $[4.5] = 23.78 \pm 0.25$ mag, and $(H - [3.6]) = 1.17 \pm 0.32$ mag. The remaining eight galaxies are undetected to $[3.6] \sim 26.4$ mag and $[4.5] \sim 26.0$ mag with stellar masses of $\sim 5 \times 10^7 M_\odot$. The detected galaxy has an estimated magnification of $\mu = 12 \pm 4$, which implies this galaxy has an ultraviolet luminosity of $L_{1500} \sim 0.3 L_{\odot}^*$ — the lowest luminosity *individual* source detected in IRAC at $z \gtrsim 7$. By modeling the broadband photometry, we estimate the galaxy has an intrinsic star-formation rate of $\text{SFR} \sim 1.3 M_\odot \text{ yr}^{-1}$ and stellar mass of $M \sim 2.0 \times 10^9 M_\odot$, which gives a specific star-formation rate of $\text{sSFR} \sim 0.7 \text{ Gyr}^{-1}$. If this galaxy had sustained this star-formation rate since $z \sim 20$, it could have formed the observed stellar mass (to within a factor of ~ 2), we also discuss alternate star-formation histories and argue the exponentially-increasing model is unlikely. Finally, based on the intrinsic star-formation rate, we estimate this galaxy has a likely [C II] flux of $\langle f_{[\text{C II}]} \rangle = 1.6 \text{ mJy}$.

Subject headings: Keywords: galaxies: high-redshift — galaxies: evolution — galaxies: formation

1. INTRODUCTION

Determining the details of cosmic reionization of hydrogen at high redshift is a central question to modern cosmology. Although the observed optical depth to Thompson scattering (Hinshaw et al. 2013) and complete Gunn-Peterson troughs (Becker et al. 2001) suggest that instantaneous reionization occurred around $z \sim 10$ and was completed by $z \sim 6$, the sources responsible for the ionizing radiation are far from clear. Although dwarf galaxies are sufficiently numerous and energetic to reionize the Universe (e.g. Yan & Windhorst

2004; Bouwens et al. 2006; Sawicki & Thompson 2006; Lemaux et al. 2009), it is uncertain how the ionizing photons escape such galaxies (e.g. Shapley et al. 2006). Consequently tracing the physical properties of the dwarf galaxy population into the neutral epoch is key in understanding cosmic reionization (e.g. Fontanot, Cristiani, & Vanzella 2012), and is a primary goal for the next-generation facilities and surveys.

As the ionizing radiation is likely emitted by hot, young stars, the current star-formation rate (SFR) is of great interest (e.g. Bouwens et al. 2007). However, the conversion from ultraviolet luminosity to SFR is complicated by an unknown extinction corrections (e.g. Bouwens et al. 2010), which can be mitigated to some extent with longer wavelength data (Finkelstein et al. 2010). Although with the Infrared Array Camera (IRAC) on the Spitzer Space Telescope (SST) observations redward of the 4000 Å-break (in the restframe of high-redshift galaxies) are routinely available, new practical problems with source blending and confusion have arisen. After dealing with issues, it seems that high-redshift galaxies have $(H - [3.6]) \sim 0.6$ mag (e.g. Gonzalez et al. 2012). Naïvely, this suggests that the galaxies have strong 4000 Å-breaks indicative of an evolved population (e.g. Eyles et al. 2007), but such breaks seem unlikely given the age of the Universe at these redshifts (Richard et al. 2011). Instead this red color may point to a significant emission-line flux in the IRAC channels (Zackrisson, Bergvall, & Leitert 2008). Because both a 4000 Å-break and optical emission lines are likely present, the IRAC photometry is a critical component in modeling the spectra and determining the stellar mass, age, and SFR of high-redshift galaxies (e.g.

rryan@stsci.edu

² Space Telescope Science Institute, 3700 San Martin Dr., Baltimore, MD 21218

³ Department of Astronomy, University of Florida, 211 Bryant Space Science Center, Gainesville, FL 32611

⁴ Aix Marseille Université, CNRS, LAM (Laboratoire d'Astrophysique de Marseille) UMR 7326, 13388, Marseille, France

⁵ University of California, One Shields Ave., Davis, CA 95616

⁶ Kavli Institute for Particle Astrophysics and Cosmology, Stanford University, 452 Lomita Mall, Stanford, CA 94305-4085

⁷ Department of Astronomy and Astrophysics, University of Chicago, 5640 South Ellis Avenue, Chicago, IL 60637

⁸ Department of Physics and Astronomy, University of British Columbia, 6224 Agricultural Road, Vancouver, BC V6T 1Z1, Canada

⁹ Steward Observatory, University of Arizona, 933 N. Cherry Ave., Tucson, AZ 85721

¹⁰ Argelander Institute for Astronomy, University of Bonn, Auf dem Hügel 71, D-53121 Bonn, Germany

¹¹ Department of Physics, University of California, Santa Barbara, CA 93106

¹² Kavli Institute of Theoretical Physics, University of California, Santa Barbara, CA 93106-4030

¹³ Dark Cosmology Centre, Niels Bohr Institute, University of Copenhagen, Juliane Maries Vej 30, 2100 Copenhagen Ø, Denmark

Papovich & Bell 2002).

Many of the previous interpretations of the IRAC data of $z \gtrsim 7$ galaxies come from *stacking* fluxes of otherwise undetected, individual galaxies (e.g. Labbé et al. 2010a; Gonzalez et al. 2012; Labbé et al. 2012). In such analyses, one selects objects of comparable properties (such as H -band magnitude), and combines the IRAC data to build up the “average” signal, effectively simulating deeper data. Despite the merits, this approach has three short-comings: First, extreme or exotic objects, which may challenge existing models or skew averages, may be excluded. Second, this method implicitly assumes that one obtains a homogeneous sample of galaxies by selecting on the H -band flux. However in the case of H -band flux, this is not guaranteed since this restframe wavelength is sensitive to both present star formation and extinction. Therefore these stacked samples are essentially selected on a combination of SFR and dust extinction, which complicates the interpretation of their “average” stellar populations. Finally, narrow emission lines can be smeared out by stacking galaxies of unknown (or imprecise) redshifts, which complicates the assessment of their ionizing budget. In contrast to stacking, one can use massive clusters of galaxies as *cosmic telescopes* and magnify background objects, which makes it possible to study intrinsically fainter individual objects for the same exposure time. Indeed this approach is quickly becoming a key tool in the study of high-redshift galaxies with the implementation of the Hubble Space Telescope (HST) Frontier Fields program (HFF)¹³.

In this paper, we present the first results from the *Spitzer UltraFaint Survey: SURFS UP*, a *Spitzer* Exploratory Program (PropID: 90009; PI: M. Bradač) approved in Cycle 9 during the Warm Mission (Bradač et al. 2014). This program adds ~ 25 hr in both IRAC channels to the existing ~ 5 hr for 10 strong-lensing galaxy clusters at $0.3 \leq z \leq 0.7$. Six of these clusters are part of the Cluster Lensing and Supernova Survey with Hubble program (CLASH; Postman et al. 2012), two are scheduled for Year 2 of the HFF (MACS J0717.5+3745 and MACS J1149.5+2223), and six are planned for the Grism Lens-Amplified Survey from Space (GLASS; PI: Treu). Here we discuss z' -band dropouts lensed by the Bullet Cluster and identified by Hall et al. (2012). This paper is organized as follows: in section 2 we discuss the SST/IRAC data, in section 3 we describe our photometry and treatment of deblending, in section 4 we present the SED modeling, and in section 5 we give concluding remarks with comments for future work. We quote all magnitudes in the AB system and adopt a Λ CDM concordance cosmology ($\Omega_0 = 0.3$, $\Omega_\Lambda = 0.7$, and $H_0 = 70 \text{ km s}^{-1} \text{ Mpc}^{-1}$).

2. OBSERVATIONS

The SST/IRAC observations for the Bullet Cluster were taken as part of three programs (proposal IDs: 3550, 60034, 90009), with $\gtrsim 70\%$ coming from *SURFS UP*. A thorough description of the data reduction and survey strategy is discussed by Bradač et al. (2014), but here we give important details. We generate mosaics using the *mopex* software from the corrected-basic calibrated

data (cBCD) after applying additional mitigation measures (see Bradač et al. 2014). There are 277 frames, which we drizzled to an output scale of $0''.60 \text{ pix}^{-1}$ yielding an integration time of $\gtrsim 110$ ks per pixel in the regions near the Hall et al. (2012) z' -dropouts. We astrometrically matched these mosaics to the F160W images from Wide-Field Camera 3 (WFC3) on the *Hubble Space Telescope* (HST).

In addition to these IRAC and existing HST data, the Bullet Cluster was also observed by the *Very Large Telescope* (VLT) for 3.75 hr with the HAWK-I imager in the K_s -band (Clément et al. 2012). Although these data have good seeing ($\sim 0''.45$), none of the Hall et al. (2012) candidates are detected. Instead we derive 1σ upper limits from the recovery rate of artificial point-sources placed near the positions of the Hall et al. (2012) sources.

3. PHOTOMETRY

Given the dense cluster environment, many of the sources from Hall et al. (2012) are blended with neighboring objects, which precludes the use of simple aperture photometry, therefore we use PyGFIT (Mancone et al. 2013). We start by using GALFIT (Peng et al. 2002) to model all objects (with Sérsic or point-source profiles) for all objects detected in HST/WFC3 F160W data near the dropouts. Taking these models as input templates, we extract photometry from the IRAC 3.6 μm and 4.5 μm data. These H -band estimates are taken as the initial conditions for PyGFIT, which convolves parametric templates with a point-spread function (PSF) and simultaneously fits for fluxes of all the sources in the region of interest. We adopt the empirical PSFs presented by Bradač et al. (2014) generated by a stack of ~ 100 point sources in the field. We allow small shifts in the source coordinates to account for any residual astrometric offsets. As a final note, the photometry presented by Hall et al. (2012) were extrapolated to infinity assuming a model PSF.

To estimate the flux uncertainties from the GALFIT modeling, we run simulations in which we randomly insert point sources into the image (all dropouts are unresolved in IRAC) and compute the scatter in the output fluxes as a function of source brightness. From the modeling and simulations, we derive best fit fluxes and uncertainties for all sources from Hall et al. (2012) except for source 5, which lies at the edge of the HST field of view and in IRAC is blended with a source outside the HST footprint. We omit this galaxy in all subsequent analyses. In Table 1, we present our IRAC photometry. None of the dropouts are sufficiently close in the IRAC images to brighter sources that confusion precludes recovery of the photometry. From this image modeling, we find that only candidate 3 from Hall et al. (2012) is robustly detected — it is detected in both warm-mission bands (see Figure 1). Whereas candidate 10, which was spectroscopically confirmed to be at $z = 6.740$ (Bradač et al. 2012), is not detected in either IRAC band. For the eight undetected objects, we estimate upper limits for the IRAC fluxes by computing the RMS in a $3''$ (radius) aperture on the sky after “cleaning” the foreground objects. Our 1σ upper limits are typically $[3.6] \leq 26.4 \text{ mag}$ and $[4.5] \leq 26.0 \text{ mag}$ (see Table 1), and are not highly sensitive to the aperture size. These limits are consistent with the

¹³ <http://www.stsci.edu/hst/campaigns/frontier-fields/HDF1SWGReport2012.pdf>

TABLE 1
OBSERVED PROPERTIES

galaxy	RA (h m s)	Dec (° ′ ″)	μ	F160W [†] (mag)	[3.6] [†] (mag)	[4.5] [†] (mag)
1	06 58 37.13	−55 58 28.070	4.3 ± 0.20	26.77 ± 0.23	> 26.7	> 26.3
2	06 58 37.26	−55 58 18.844	6.5 ± 0.50	26.97 ± 0.23	> 26.5	> 26.2
3	06 58 40.17	−55 58 05.041	12 ± 4.00	24.97 ± 0.16	23.80 ± 0.28	23.78 ± 0.25
4	06 58 39.30	−55 55 43.687	2.8 ± 0.08	26.37 ± 0.22	> 26.5	> 26.1
5	06 58 32.25	−55 58 42.971	2.1 ± 0.03	25.91 ± 0.22
6	06 58 29.87	−55 57 03.834	$10. \pm 2.00$	25.85 ± 0.19	> 26.4	> 26.1
7	06 58 34.33	−55 57 53.122	5.2 ± 0.50	25.81 ± 0.26	> 26.6	> 26.2
8	06 58 34.92	−55 55 29.381	3.1 ± 0.10	25.89 ± 0.21	> 26.6	> 26.2
9	06 58 31.81	−55 57 49.550	4.3 ± 0.30	26.00 ± 0.16	> 26.6	> 26.2
10	06 58 31.24	−55 58 13.735	3.0 ± 0.20	26.37 ± 0.16	> 25.8	> 24.5

–The upper limits for [3.6] and [4.5] are 1σ .

[†]These quantities have *not* been corrected for the magnification (μ).

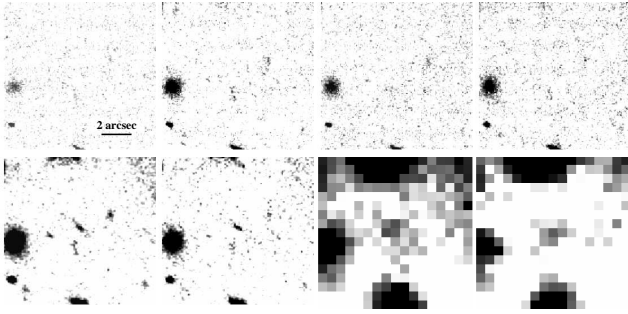


FIG. 1.— HST and SST imaging. Here we show the eight images for candidate 3 from Hall et al. (2012). Each stamp is $10''$ on a side and north-up and east-left. The top row shows the non-detections from HST in F606W, F775W, F814W, and F850LP, respectively. The bottom row shows the detections from HST and SST in F110W, F160W, [3.6], and [4.5], respectively. This object is robustly detected in both IRAC bands and reasonably isolated from any neighboring object.

exposure-time calculator estimates Bradač et al. (2014) and only account for the sky noise in the vicinity of the dropouts. Therefore these limits are ~ 1 mag deeper than the artificial source tests, which additionally include uncertainties associated with confusion, blending, and overlapping sources.

4. SED MODELING AND PHOTOMETRIC REDSHIFTS

For each candidate, we fit the combined nine-band photometry from HST, VLT, and SST using *Le Phare* (Ilbert et al. 2006, 2009). We use 27 stellar population synthesis models generated using Bruzual & Charlot (2003, hereafter BC03) models at 58 ages that range from 0.1 – 13.5 Gyr and exclude ages greater than the age of the Universe¹⁴. These BC03 models use a Chabrier (2003) initial mass function (IMF) with metallicities of $Z = (0.02 - 1) Z_{\odot}$ and are characterized by exponentially-declining star-formation histories (SFHs) with timescales of $\tau = 0.1 - 30$ Gyr. We adopt the Calzetti et al. (2000) reddening law with $0 \leq E(B - V) \leq 0.5$. In addition, *Le Phare* adds nebular emission lines to the BC03 templates using a direct translation between the dust-corrected ultraviolet (UV) luminosity at rest-frame 2300 Å and the [O II] $\lambda 3727$ Å feature, which is subsequently used to derive the strength of other rest-frame

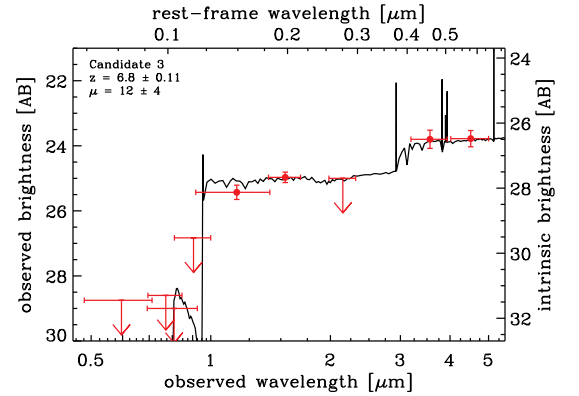


FIG. 2.— SED fit for candidate 3. Here the red points show the observed photometry from HST/VLT/SST (the upper limits are 1σ), and the black line is the best-fit model from *Le Phare* (including emission lines Ilbert et al. 2009). On the right vertical axis, we show the *intrinsic* apparent magnitudes ($m_{\text{inst}} = m_{\text{obs}} + 2.5 \log \mu$) to demonstrate the effect of the lensing. The horizontal error bars represent the FWHM and the points are placed at the mean wavelength of each band. For this object, we obtain a photometric redshift of $z = 6.8^{+0.12}_{-0.10}$ which gives an FUV luminosity of $L_{1500} \sim 0.3 L_{*}^{\text{FUV}}$, the lowest-luminosity source at $z \gtrsim 6$ yet detected by SST/IRAC. Constraining the SFR of such low-luminosity galaxies is critical in establishing the ionizing flux budget.

UV/optical emission features using average intrinsic ratios (see Ilbert et al. 2009). *Le Phare* estimates the current SFR from dust-corrected UV luminosity and standard relations (Kennicutt 1998). To estimate parameter uncertainties, we add Gaussian noise to each photometric point for each galaxy, re-fit with *Le Phare*, and compute the RMS of best-fit parameters. In Table 2, we present the best-fit SED parameters for the Hall et al. (2012) z' -dropouts and show the SED fit for the IRAC-detected object in Figure 2.

In Figure 3 we show the distribution of SED parameters for the object 3, which was detected in both IRAC channels. The open and shaded histograms show the results with and without the inclusion of the IRAC data, respectively. The rest-frame optical data help markedly in constraining the age and stellar mass, whereas they have less effect on the redshift or the precision of the SFR rate. This is not surprising because much of the redshift information is encapsulated in the observed Lyman break between the z' - and J -bands, whereas the age and stel-

¹⁴ At $z \sim 7$ the age of the Universe is ~ 760 Myr.

TABLE 2
STELLAR POPULATION RESULTS

gal	z	$\log t$ (yr)	$\log M^\dagger$ (M_\odot)	$\log \text{SFR}^\dagger$ ($M_\odot \text{ yr}^{-1}$)	E_{B-V} (mag)
1	$6.5^{+0.30}_{-0.20}$	$7.6^{+0.55}_{-0.58}$	$7.9^{+0.20}_{-0.28}$	$0.24^{+0.34}_{-0.34}$	$0.10^{+0.1}_{-0.1}$
2	$6.4^{+0.17}_{-0.27}$	$7.7^{+0.81}_{-0.68}$	$7.7^{+0.33}_{-0.62}$	$-0.10^{+0.62}_{-0.34}$	$0.0^{+0.2}_{-0.0}$
3	$6.8^{+0.12}_{-0.10}$	$8.8^{+0.10}_{-0.20}$	$9.3^{+0.11}_{-0.23}$	$0.12^{+0.31}_{-0.28}$	$0.0^{+0.4}_{-0.0}$
4	$7.9^{+0.065}_{-0.87}$	$7.5^{+0.38}_{-0.46}$	$8.1^{+0.19}_{-0.23}$	$0.56^{+0.41}_{-0.21}$	$0.0^{+0.1}_{-0.0}$
5	omitted from this analysis				
6	$7.1^{+0.75}_{-0.10}$	$7.0^{+0.72}_{-0.00}$	$7.3^{+0.065}_{-0.06}$	$0.22^{+0.054}_{-0.08}$	$0.0^{+0.1}_{-0.0}$
7	$7.0^{+1.0}_{-0.10}$	$7.0^{+0.89}_{-0.00}$	$7.4^{+0.041}_{-0.06}$	$0.43^{+0.041}_{-0.08}$	$0.0^{+0.1}_{-0.0}$
8	$6.9^{+1.1}_{-0.40}$	$7.0^{+1.0}_{-0.00}$	$7.7^{+0.16}_{-0.08}$	$0.61^{+0.077}_{-0.12}$	$0.0^{+0.1}_{-0.0}$
9	$7.8^{+0.17}_{-0.58}$	$7.0^{+0.38}_{-0.00}$	$7.6^{+0.13}_{-0.06}$	$0.52^{+0.076}_{-0.12}$	$0.0^{+0.1}_{-0.0}$
10*	6.740^*	$7.7^{+0.65}_{-0.63}$	$8.1^{+0.55}_{-0.51}$	$0.43^{+0.26}_{-0.19}$	$0.0^{+0.3}_{-0.0}$

The SFRs presented here was derived with *Le Phare*, and is similar to the calculation discussed in § 5.

*For this object, the redshift was fixed to the spectroscopic value (Bradač et al. 2012).

†These quantities have been corrected for the magnification (μ , see Table 1).

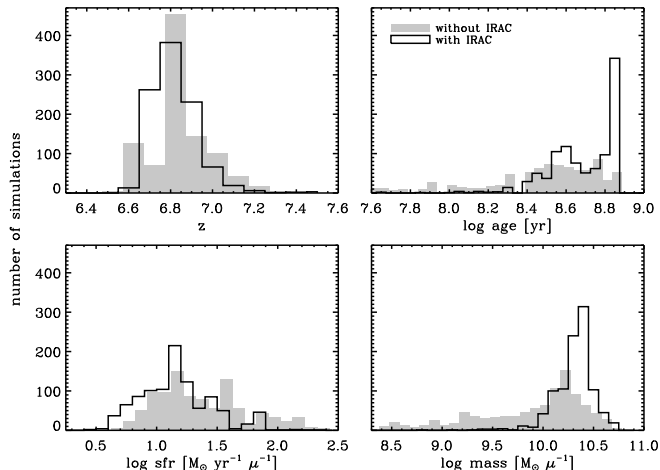


FIG. 3.— Stellar population parameters for candidate 3. To estimate the uncertainty on these parameters, we use a simple Monte Carlo simulation where we fit each galaxy 1000 times with the fluxes tweaked by their uncertainties. The open histogram shows results for the nine-band photometry from HST/VLT/SST. To illustrate the importance of the IRAC data in modeling these galaxies, we show the results without the IRAC data (shaded histogram, we slightly offset the shaded histograms for clarity). The redshift is robust to the exclusion of the IRAC data, whereas the SFR is ~ 2 times higher without IRAC and stellar mass is almost completely uncertain.

lar mass depend critically on the 4000 \AA break and the rest-frame optical data. Finally, it is becoming widely accepted that optical emission lines ($\text{H}\beta$, $[\text{O III}]$, $\text{H}\alpha$) contribute a significant flux to the IRAC bands. However, object 3 seems to be a unique redshift where the additional flux from $\text{H}\beta$ and $[\text{O III}]$ is offset by a slightly lower continuum, giving a fairly “neutral” IRAC color. Using a set of fixed equivalent widths: $\text{EW}_{\text{rest}}(\text{H}\beta, [\text{O III}], \text{H}\alpha) = (105, 670, 300) \text{ \AA}$, Gonzalez et al. (2012) show that emission lines contribute little to the observed $([3.6] - [4.5])$ color. Therefore the equivalent widths of these emission lines in object 3 are likely no larger than the Gonzalez et al. (2012) assumptions.

5. DISCUSSION

We have presented the first results from SURFS UP¹⁵, a Spitzer Exploration Program to image 10 strong-lensing clusters to $\sim 100 \text{ ks}$ depth per channel. We have definitively detected one of the 10 z' -band dropouts identified by Hall et al. (2012). This galaxy is highly magnified by the Bullet Cluster ($\mu = 12 \pm 4$) with an apparent magnitude of $J = 25.43 \pm 0.22 \text{ mag}$, which gives a far-UV luminosity of $M_{1500} = -18.9 \pm 0.42 \text{ mag}$ (accounting for both the photometric and magnification uncertainty). Therefore this galaxy has $L_{1500} \sim 0.3 L^*$ (taking $M_{1500}^* = -20.14 \text{ mag}$ from Bouwens et al. 2011), and is the only *individual* dwarf galaxy at $z \gtrsim 7$ detected so far by IRAC (c.f. Yan et al. 2012; Labbé et al. 2012). This is the first direct detection of the kind of galaxy likely responsible for the cosmic reionization. From the SED modeling we infer a specific star-formation rate (sSFR) of $\text{sSFR} \sim 0.7 \text{ Gyr}^{-1}$, which is lower than comparable galaxies (e.g. Zheng et al. 2012; Zitrin et al. 2012) or at low redshift (e.g. Noeske et al. 2007). In contrast, the remaining eight galaxies have $\langle \text{sSFR} \rangle \sim 50 \text{ Gyr}^{-1}$, similar to Lyman-break galaxies (LBGs) at $z \sim 5$ (Hathi et al. 2012), suggesting that this detected object may be an unusual member of the high-redshift galaxy population.

It is intriguing to consider the SFHs that could yield a substantial stellar mass ($M_* \sim 2^{+0.6}_{-0.9} \times 10^9 M_\odot$) at this early epoch. The two inferences of stellar mass and SFR essentially constrain the integral and current value of the SFH, respectively. Assuming that galaxies begin to form around $z_{\text{form}} \sim 20$, then this galaxy must have acquired the observed stellar mass in $\lesssim 650 \text{ Myr}^{16}$. If it had constantly formed stars at the measured rate over this time, then it would have built up a stellar mass of $8.4 \times 10^8 M_\odot$. Although this constant SFR model is roughly consistent with the derived mass ($\sim 1.5 \sigma$), it suggests that the SFR could not have been lower in the past without some corresponding period of increased star formation. Of course it is impossible to distinguish between a smooth, multi-component SFH (e.g. Lee et al. 2010; Behroozi, Wechsler, & Conroy 2013; Pacifici et al. 2013) from a stochastic history punctuated by intense bursts. But, it does imply that the exponentially-increasing model (Maraston et al. 2010) can be ruled out, given its substantial stellar mass, modest SFR, and high redshift. If the actual formation redshift were lower than our conservative assumption, then the argument becomes stronger as the constant star-formation scenario cannot create enough mass by $z \sim 7$.

In the above we tacitly assumed that the stellar mass was created *in situ*, and that it had not experienced any type of merger. Although mergers would bring in stellar mass (and possibly enhance the star formation), they are not on frequent enough to change the mass significantly (Hopkins et al. 2010). Using their merger rate calculator, we estimate that a galaxy with a stellar mass of $2 \times 10^9 M_\odot$ will have an average major merger rate of $\sim 0.9 \text{ mergers Gyr}^{-1}$. In the $600 - 700 \text{ Myr}$ available to this galaxy (the range reflects the $\pm 3\sigma$ uncertainty on

¹⁵ <http://www.physics.ucdavis.edu/~marusa/SurfsUp.html>

¹⁶ Although we estimate the age in Table 2, this age is indicated on an exponentially-declining SFH. To avoid circularity in the argument, we instead adopt a conservative estimate for the formation redshift.

the photometric redshift), there are only 0.5–0.7 mergers of mass ratio $0.25 < m_1/m_2 < 1$. Even if major mergers contributed to the observed stellar mass of this galaxy, this scenario raises the question of how two progenitors with stellar masses of $M_* \sim 10^9 M_\odot$ formed — the one galaxy is puzzling enough. While this galaxy may have had an exceptionally high merger rate, the major merger scenario seems unlikely, which leaves minor mergers or gradual accretion/inflow a possibility. Certainly gas inflow is an early prediction for the formation of the earliest galaxies (e.g. Larson 1972) and has even been observed in low-redshift star-forming galaxies (Rubin et al. 2012). Our broadband data are insensitive to the observational signatures of inflow (such as redshifted resonance lines; Martin et al. 2012), but it possible with the *The James Webb Space Telescope*.

We estimate this galaxy has an observed SFR = $16_{-8}^{+16} \mu^{-1} M_\odot \text{ yr}^{-1}$, and is a prime candidate for follow-up with the Atacama Large Millimeter Array (ALMA). Like the far-ultraviolet (FUV), the far-infrared (FIR) has many useful SFR indicators, particularly the [C II] $\lambda 157.7 \mu\text{m}$ emission line and thermal continuum from warm dust. To predict the [C II] flux, we use the SFR estimated in Section 4 and calibrations from de Looze et al. (2011), to predict an integrated line flux of $F_{[\text{C II}]} \sim 10^{-17} \text{ erg s}^{-1} \text{ cm}^{-2}$. If we assume a Gaussian line profile (of width $\Delta v = 100 \text{ km s}^{-1}$), the SFR gives an average flux density of $\langle f_{[\text{C II}]} \rangle = 1.6 \text{ mJy}$. Because our SED models imply a small amount of dust (see Table 2) and recent chemical evolution models find a sufficient amount of dust can be produced by $z \sim 6$ (Valiante et al. 2009), we estimate the FIR continuum flux (8–1000 μm) using the Kennicutt (1998) scaling relation. We predict this galaxy will have an integrated flux of $F_{\text{FIR}} = 4 \times 10^{-15} \text{ erg s}^{-1} \text{ cm}^{-2}$, which averaged over 8–1000 μm is $\langle f_{\text{FIR}} \rangle = 12 \mu\text{Jy}$. All fluxes discussed in this paragraph include the magnification. These flux levels are readily achievable, even with the current ALMA facilities (e.g. Waggoner et al. 2012).

Using standard tools and techniques we have robustly detected 1/9 z' -dropouts from Hall et al. (2012). For the remaining eight galaxies that have gone undetected in SURFS UP we performed a similar tweaking/re-fitting

analysis described in section 4. We tweak the IRAC upper limits for the eight undetected galaxies slightly deeper ($\sim 0.25 \text{ mag}$) and re-fit with *Le Phare*. We find that either no combination of physical parameters could effectively characterize the tweaked photometry or that resulting best-fit models required extreme properties: very young ages ($\lesssim 10 \text{ Myr}$) or low stellar masses ($\lesssim 10^8 M_\odot \mu^{-1}$; where μ is the magnification). As such, we suspect that the IRAC limits quoted in Table 1 for the remaining eight galaxies (where one is unobservable as discussed in section 3) are close to their true brightnesses. As part of our on-going efforts with SURFS UP we will continue to develop tools and techniques to deal with the unique challenges posed by this and similar datasets.

We would like to thank the anonymous Referee for several insightful suggestions and comments. We also recognize Olivier Ilbert, Steve Finkelstein, Seth Cohen, Norman Grogan, Jen Lotz, and Preethi Nair for their helpful discussions. The HAWK-I K -band data was provided by B. Clement, and was taken as part of the ESO Large Program ID: 181.A-0485 (PI: J. G. Cuby). This work is based [in part] on observations made with the Spitzer Space Telescope, which is operated by the Jet Propulsion Laboratory, California Institute of Technology under a contract with NASA. Support for this work was provided by NASA through an award issued by JPL/Caltech and through HST-GO-10200, HST-GO-10863, and HST-GO-11099 from STScI. TT acknowledges support by the Packard Fellowship. Part of the work was carried out by MB and TT while attending the program “First Galaxies and Faint Dwarfs” at KITP which is supported in part by the NSF under Grant No. NSF PHY11-25915. TS acknowledges support from the German Federal Ministry of Economics and Technology (BMWi) provided through DLR under project 50 OR 1308. HH is supported by the DFG grant Hi 1495/2-1. SA and AvdL acknowledge support by the U.S. DoE under contract number DE-AC02-76SF00515 and by the Dark Cosmology Centre which is funded by the Danish National Research Foundation.

Facilities: SST (IRAC)

REFERENCES

- Becker, R. H., et al. 2001, *AJ*, 122, 2850
 Behroozi, P. S., Wechsler, R. H., & Conroy, C. 2013, *ApJ*, 770, 47
 Bouwens, R. J., Illingworth, G. D., Blakeslee, J. P., & Franx, M. 2006, *ApJ*, 653, 53
 Bouwens, R. J., Illingworth, G. D., Franx, M., & Ford, H. 2007, *ApJ*, 670, 928
 Bouwens, R. J., et al. 2010, *ApJ*, 708, L69
 Bouwens, R. J., et al. 2011, *ApJ*, 737, 33
 Bradač, M., et al. 2012, *ApJ*, 755, L7
 Bradač, M., et al. 2013, *ApJ*, accepted
 Bruzual, G. & Charlot, S. 2003, *MNRAS*, 344, 1000 (BC03)
 Calzetti, D., Armus, L., Bohlin, R. C., Kinney, A. L., Koornneef, J., & Storchi-Bergmann, T. 2000, *ApJ*, 533, 682
 Chabrier, G. 2003, *PASP*, 115, 763
 Clément, B., et al. 2012, *A&A*, 538, 66
 de Looze, I., Baes, M., Bendo, G. J., Cortese, L., & Friz, J. 2011, *MNRAS*, 416, 2712
 Eyles, L. P., Bunker, A. J., Ellis, R. S., Lacy, M., Stanway, E. R., Stark D. P., & Chiu K. 2007, *MNRAS*, 374, 910
 Finkelstein, S. L., Papovich, C., Giavalisco, M., Reddy, N. A., Ferguson, H. C., Koekemoer, A. M., & Dickinson, M. E. 2010, 719, 1250
 Fontanot, F., Cristiani, S., & Vanzella, E. 2012, *MNRAS*, 425, 1413
 Gonzalez, V., Bouwens, R., Labbé I., Illingworth, G., Oesch, P., Franx, M., & Magee, D. 2012, *ApJ*, 755, 148
 Hall, N., et al., 2012, *ApJ*, 745, 155
 Hathi, N. P., et al. 2013, *ApJ*, 765, 88
 Hinshaw, G., et al. 2013, *ApJS*, 208, 19
 Hopkins, P. F., et al. 2010, *ApJ*, 715, 202
 Ilbert, O., et al. 2006, *A&A*, 457, 841
 Ilbert, O., et al. 2009, *ApJ*, 690, 1236
 Kennicutt, R. G. 1998, *ARA&A*, 36, 189
 Labbé, I., et al. 2010, *ApJ*, 716, L103
 Labbé, I., et al. 2012, *arXiv*: 1209.3037
 Larson, R. 1972, *Nature*, 236, 21
 Lee, S.-K., Ferguson, H. C., Somerville, R. S., Wiklind, T., & Giavalisco, M. 2010, *ApJ*, 725, 1644
 Lemaux, B. C., et al. 2009, *ApJ*, 700, 20
 Madau, P., Pozzetti, L., & Dickinson, M. 1998, *ApJ*, 498, 106
 Makovoz, D., Khan, I., & Moshir, M. 2005, *PASP*, 117, 274
 Mancone, C. L., Gonzalez, A. H., Moustakas, L. A., & Price, A. 2013, *PASP*, accepted (*arXiv*: 1310.6046)

- Maraston, C., Pforr, J., Renzini, A., Daddi, E., Dickinson, M., Cimatti, A., & Tonini, C. 2010, *MNRAS*, 407, 830
- Martin, C. L., Shapley, A. E., Coil, A. L., Kornei, K. A., Bundy, K., Weiner, B. J., Noeske, K. G., & Schiminovich, D. 2012, *ApJ*, 760, 127
- Noeske, K. G., et al. 2007, *ApJ*, 660, L43
- Pacifici, C., Kassim, S. A., Weiner, B., Charlot, S., & Gardner, J. P. 2013, 762, L15
- Papovich, C. & Bell, E. F. 2002, *ApJ*, 579, L1
- Peng, C. Y., Ho, L. C., Impey, C. D., & Rix, H.-W. 2002, *AJ*, 124, 266
- Postman, M., et al. 2012, *ApJS*, 199, 25
- Richard, J., Kneib, J.-P., Ebeling, H., Stark, D. P., Egami, E., & Fiedler, A. K. 2011, *MNRAS*, 414, L31
- Rubin, K. H. R., Prochaska, J. X., Koo, D. C., & Phillips, A. C. 2012, *ApJ*, 747, L26
- Sawicki, M. & Thompson, D. 2006, *ApJ*, 648, 299
- Shapley, A. E., Steidel, C. C., Pettini, M., Adelberger, K. L., & Erb, D. K. 2006, *ApJ*, 651, 688
- Valiante, R., Schneider, R., Bianchi, S., & Andersen, A. C. 2009, *MNRAS*, 397, 1661
- Wagg, J., et al. 2012, *ApJ*, 752, L30
- Yan, H. & Windhorst, R. A. 2004, *ApJ*, 600, L1
- Yan, H., et al. 2012, *ApJ*, 761, 177
- Zackrisson, E., Bergvall N., & Leitert, E. 2008, *ApJ*, 676, L9
- Zheng, W., et al. 2012, *Nature*, 489, 406
- Zitrin, A., et al. 2012, *ApJ*, 747, L9